J. Math. Biol. 47, 424–452 (2003)
Digital Object Identifier (DOI):
10.1007/s00285-003-0214-x

Mathematical Biology

S.J. Franks · H.M. Byrne · J.R. King · J.C.E. Underwood · C.E. Lewis

Modelling the early growth of ductal carcinoma in situ of the breast

Received: 3 July 2002 / Revised version: 26 February 2003 /
Published online: 15 May 2003 –

Abstract. The growth of a tumour in a rigid walled cylindrical duct is examined in order to model the initial stages of tumour cell expansion in ductal carcinoma in situ (DCIS) of the breast. A nutrient-limited growth model is formulated, in which cell movement is described by a Stokes flow constitutive relation. The effects on the shape of the tumour boundary of the material properties (i.e. the viscosity) and the extent to which the cells adhere to the duct wall are studied using numerical and asymptotic methods. It is shown how stable, non-planar, interface configurations result and that, during these initial stages, before the duct wall has been breached, few cells die and a nutrient-rich model is usually sufficient to capture the behaviour. Finally, we discuss the relevance of this approach to DCIS and suggest possible avenues for further work.

1. Introduction

Breast cancer is the most common cancer in women, among whom it is the second leading cause of cancer death. Ductal carcinoma in situ (DCIS) of the breast represents the initial growth stage of breast cancer. At this stage, the tumour is noninvasive, being confined by the basement membrane of the duct. However, if left untreated, it is thought to then invade the breast stromal tissue surrounding the ducts and become life threatening. The duct is made up of a central region of lumen (extracellular fluid), lined by a thin layer of epithelial cells, a layer of myo-epithelial cells and an outer basement membrane (the duct wall) comprising a meshwork of proteins. Ducts in the healthy breast have an average diameter of 0.2mm and are surrounded by stroma (connective tissue). DCIS occurs when there is a proliferation of epithelial cells that have undergone a malignant transformation (usually originating from a single mutant cell).

DCIS is characterised according to the appearance of the tumour cells proliferating within the duct and the broadest classification subdivides them into two types: high (comedo) and low grade (cribriform) DCIS [15]. Low grade DCIS is

S.J. Franks, H.M. Byrne, J.R. King: Centre for Mathematical Medicine, School of Mathematical Sciences, University of Nottingham, Nottingham NG7 2RD, UK.
e-mail: susan.franks@nottingham.ac.uk

S.J. Franks, J.C.E. Underwood, C.E. Lewis: Division of Genomic Medicine, University of Sheffield Medical School, Beech Hill Road, Sheffield S10 2RX, UK

Send offprint requests to: S.J. Franks at Centre of Mathematical Medicine.

Key words or phrases: DCIS – Stokes flow – Nutrient-limited growth – Slender approximation – Stability

well differentiated (where the degree of differentiation refers to the loss of normal tissue organisation) and appears homogeneous. Necrosis is rarely present as the duct typically only distends to an average diameter of about 0.4mm. Thus, even though the stromal vessels are smaller and fewer in number than for high grade DCIS, all cells receive an adequate supply of nutrient by diffusion from surrounding vessels. High grade DCIS is poorly differentiated, with cells proliferating and dying at elevated rates. The duct tends to be very large and distended, with an average diameter of about 0.7mm and comprises an outer proliferating rim, a region of viable, non-proliferating hypoxic cells and a central necrotic core. There is an increase in the number of stromal vessels surrounding the duct and a higher risk of progression to breast cancer than the low grade type [10].

If DCIS is to progress to breast cancer, cancer cells must penetrate the basement membrane and force their way through the surrounding stroma [3]. Continued tumour cell proliferation in the duct gradually increases the outward pressure on the basement membrane which, together with the local production of proteolytic enzymes, causes it to yield and allows tumour cells to invade into the stroma surrounding the duct [3].

DCIS tends to be avascular as stromal vessels do not enter the duct before the tumour cells have breached the duct wall. While the growth of avascular tumours has been studied by many authors including Greenspan, Byrne, Chaplain and Please [13]–[14], [4]–[9], [21], in this paper we adopt the approach developed in [22] and [12]. In [22], Ward and King assume that the tumour is radially symmetric and consists of a continuum of live and dead cells. Local volume changes, due to cell growth and death, create cell movement which is described by a velocity field. Ward and King were able to capture the early growth and developing spatial composition of the tumour without making *a priori* assumptions about its structure. Franks and King [12] extended Ward and King's model by considering a two-dimensional tumour slab growing into surrounding tissue. A constitutive law defining the material deformation was needed in order for the problem to be completely specified. The dependence of the stability of a planar tumour surface on the material properties of the tumour and surrounding tissue was examined. Two alternative constitutive laws were used to describe the material deformation, namely Darcy's law and Stokes flow. Darcy's law has been widely used in tumour modelling ([7], [12]–[14], [17] for example) and describes fluid flow in a porous medium, relating the velocity to the pressure gradient resulting in part from the birth of new cells. By contrast, Stokes flow [12] treats the tumour and surrounding tissue as viscous, Newtonian fluids. Physically, tissue is typically modelled as a viscoelastic fluid, but on the long time scales of interest here, elastic effects are negligible so that Stokes flow provides an appropriate description. Alternative approaches to avascular tumour modelling involving multi-phase models, different constitutive relations and inhibitor effects are described in the papers by Chaplain and Sleeman [9], Byrne and Chaplain [2]–[8], Please et al. [21] and Landman and Please [17].

In this paper we extend some of the approaches used in [22] and [12] to the cylindrically-symmetric geometry of the breast duct. We assume that the duct is a rigid walled cylinder (neglecting details of its structure) and that growth occurs

only in the axial direction. We thereby seek to gain insight into the initial stages of the carcinoma's development in the duct, it being supposed that the tumour will initially grow preferentially in the direction of least resistance i.e. down the duct, rather than pushing out against the duct wall. We describe the tumour's growth using a nutrient-limited model in which the birth and death of cells is dependent upon the concentration of a nutrient which is available by diffusion from the surroundings (outside of the duct and from the fluid within the duct). We consider an axisymmetric tumour which starts as a short cylinder of the same radius as the duct, thereby avoiding the complications of treating a fully three dimensional problem. The two-dimensional tumour growing in a cylinder constrained by a rigid wall is a novel aspect of this paper.

In Section 2, we derive the mathematical model that governs the evolution of the tumour in the duct and solve the resulting system of equations numerically. In Section 3, we consider the limit where the tumour surface is defined by a sharp interface and assume that the tumour is growing in nutrient-rich conditions. We use this assumption in Sections 4 and 5 where we examine the slender approximation limit and determine the stability of the tumour surface. In the final section we discuss our conclusions and suggest extensions to the model.

2. Tumour growth model

2.1. Model formulation

Following [22], we assume that the tumour's growth is dependent upon a generic nutrient, the cells dividing and growing at a rate dependent upon the nutrient concentration. The nutrient diffuses in through the basement membrane from the vessels surrounding the duct. The birth and death of cells creates an internal velocity field and we use Stokes law to describe this deformation of the tumour region and the surrounding fluid. We denote the concentrations of live tumour cells, dead cells and surrounding material (lumen which is assumed to be like water in consistency) by $n(\mathbf{x}, t)$, $m(\mathbf{x}, t)$ and $\rho(\mathbf{x}, t)$, respectively, the nutrient concentration by $c(\mathbf{x}, t)$ and the internal velocity field (local velocity of the cells) by $\mathbf{v}(\mathbf{x}, t)$, where $\mathbf{v} = (u(\mathbf{x}, t), v(\mathbf{x}, t))$ and $\mathbf{x} = (r, z)$, r and z being the distances in the radial and axial directions, respectively, and t the time. Applying the principle of mass balance to each cell type we obtain the following partial differential equations:

$$\frac{\partial n}{\partial t} + \nabla \cdot (n\mathbf{v}) = (k_m(c) - k_d(c))n + D_n \nabla^2 n, \tag{1}$$

$$\frac{\partial m}{\partial t} + \nabla \cdot (m\mathbf{v}) = k_d(c)n + D_m \nabla^2 m, \tag{2}$$

$$\frac{\partial \rho}{\partial t} + \nabla \cdot (\rho\mathbf{v}) = D_\rho \nabla^2 \rho. \tag{3}$$

The tumour is viewed as a coherent mass whose behaviour is similar to that of a viscous fluid. Whilst cells may exhibit some small amount of random motion, the growth-driven velocity field is the dominant mechanism for their movement and the diffusion terms are included primarily for numerical purposes (to smooth out

the discontinuity at the surface by eliminating the moving boundary which would otherwise require tracking). The constants D_n, D_m and D_ρ are therefore, in effect, the diffusion coefficients of live tumour cells, dead cells and surrounding material, respectively (they will be set small and equal in the remainder of this paper). The rates of cell mitosis $k_m(c)$ and cell death $k_d(c)$ are assumed to depend on the nutrient concentration in the following manner

$$k_m(c) = Ac, \qquad k_d(c) = B\,(1 - \sigma c)\,,$$

where A and B are positive constants and $0 \leq \sigma < c_I^{-1}$ (where c_I is the external nutrient concentration) so that $k_d > 0$ for all values of c, to account for cell death due to apoptosis.

We assume that the material forms an incompressible, continuous fluid, with no voids present, so that

$$n + m + \rho = 1. \tag{4}$$

The avascular tumour obtains the necessary nutrients from the surrounding lumen and stromal tissue. The distribution of nutrient is governed by diffusion into the interior through the tumour surface and duct wall, and consumption by proliferating malignant cells within the duct. We therefore adopt the following relation.

$$\frac{\partial c}{\partial t} + \nabla \cdot (c\mathbf{v}) = D\nabla^2 c - \beta k_m(c) n, \tag{5}$$

where $\beta k_m(c)n$ represents the rate of nutrient consumption during mitosis and the diffusion coefficient D is taken to be constant.

Adding equations (1)-(3) and using (4) (and taking $D_n = D_m = D_\rho$) we deduce that the velocity field satisfies

$$\nabla \cdot \mathbf{v} = k_m(c) n \tag{6}$$

and hence that the tumour's rate of expansion is determined by the rate at which cells are being produced by mitosis.

Since the system is multi-dimensional we require a constitutive law for the material deformation (i.e. (6) is not sufficient to determine the velocity field fully). While Darcy's law has been widely used in tumour modelling, we adopt Stokes law (with a volumetric source due to cell division) which represents slow viscous flow and relates the stress experienced by the cells to their rate of strain [12] and appears more appropriate in the current context. The stress tensor σ_{ij} is given by the constitutive law

$$\sigma_{ij} = -p\delta_{ij} + 2\mu(e_{ij} - \frac{1}{3}\triangle\delta_{ij}),$$

in which the pressure $p = -\frac{1}{3}\sigma_{kk}$, the rate of strain tensor e_{ij} and the dilation $\triangle$ are defined by

$$e_{ij} = \frac{1}{2}\left(\frac{\partial u_i}{\partial x_j} + \frac{\partial u_j}{\partial x_i}\right), \qquad \triangle = e_{kk},$$

and μ is the viscosity. Since the tumour consists only of live and dead tumour cells ($n+m=1$, $\rho=0$) and the exterior, only of surrounding fluid ($n+m=0$, $\rho=1$), we assume that the viscosity depends solely on the type of material present, so $\mu=\mu(n+m)$ i.e. $\mu(1)$ is the viscosity of the tumour and $\mu(0)$ that of the surrounding material. In this context the viscosity represents the resistance to motion experienced by the cells, this being related to the strength of the bonds that hold them together which is, in turn, likely to be determined by the degree of differentiation of the tumour cells [12]. The momentum equations (with negligible inertia and no body forces [1]) read

$$\frac{\partial \sigma_{ij}}{\partial x_j}=0.$$

Substituting σ_{ij} into the momentum equations gives the Stokes equations:

$$\begin{aligned}\frac{\partial p}{\partial r}&=\mu\left(\nabla^2 u-\frac{u}{r^2}+\frac{1}{3}\frac{\partial}{\partial r}(\nabla\cdot\mathbf{v})\right)+\frac{4}{3}\frac{\partial\mu}{\partial r}\left(\frac{\partial u}{\partial r}-\frac{1}{2}\left(\frac{u}{r}+\frac{\partial v}{\partial z}\right)\right)\\&\quad+\frac{\partial\mu}{\partial z}\left(\frac{\partial u}{\partial z}+\frac{\partial v}{\partial r}\right)\end{aligned}\tag{7}$$

$$\begin{aligned}\frac{\partial p}{\partial z}&=\mu\left(\nabla^2 v+\frac{1}{3}\frac{\partial}{\partial z}(\nabla\cdot\mathbf{v})\right)+\frac{4}{3}\frac{\partial\mu}{\partial z}\left(\frac{\partial v}{\partial z}-\frac{1}{2}\left(\frac{u}{r}+\frac{\partial u}{\partial r}\right)\right)\\&\quad+\frac{\partial\mu}{\partial r}\left(\frac{\partial u}{\partial z}+\frac{\partial v}{\partial r}\right).\end{aligned}\tag{8}$$

We have now formulated the mathematical model. There are seven dependent variables (n, m, ρ, c, u, v and p) whose evolution is determined by equations (1)-(3) and (5)-(8). By noting that equations (1), (5)-(8) are independent of m and ρ we can decouple them from the other variables, with $m+\rho$ given by (4). We are essentially assuming that the tumour is a two-phase medium consisting of live and dead tumour cells and that the surrounding fluid is a single phase medium.

To complete the system, appropriate initial and boundary conditions must be specified. We assume that at $t=0$, the tumour is a cylinder of some specified width $z=s(r,0)$ and of radius $r=h$, so that

$$n(\mathbf{x},0)=\begin{cases}1 & 0<z<s(r,0),\\ 0 & z>s(r,0),\end{cases}\qquad c(\mathbf{x},0)=c_I,\tag{9}$$

where c_I is the external nutrient concentration. Boundary conditions are given by

$$\begin{aligned}&\text{on } z=0 \quad \frac{\partial n}{\partial z}=0,\ \ \frac{\partial p}{\partial z}=0,\ \ \frac{\partial u}{\partial z}=0,\ \ v=0,\ \ \frac{\partial c}{\partial z}=0,\\&\text{as } z\to\infty\ n=0,\ \ u=0,\ \ \frac{\partial v}{\partial z}=0,\ \ c=c_I,\\&\text{on } r=0 \quad \frac{\partial n}{\partial r}=0,\ \ \frac{\partial p}{\partial r}=0,\ \ u=0,\ \ \frac{\partial v}{\partial r}=0,\ \ \frac{\partial c}{\partial r}=0,\\&\text{on } r=h \quad \frac{\partial n}{\partial r}=0,\ \ u=0,\ \ \mu\frac{\partial v}{\partial r}=-\lambda v,\ \ c=c_I.\end{aligned}\tag{10}$$

The tumour is symmetric about $z = 0$ and $r = 0$ so that zero flux conditions hold and the cellular material has zero axial velocity and radial velocity, respectively. As $z \to \infty$ along the duct, the concentration of tumour cells tends to zero and the nutrient concentration takes some constant value c_I. On the rigid wall, $r = h$, the nutrient concentration is also constant, the radial velocity is zero and the axial velocity satisfies a slip condition so that the shear stress is equal to the product of the coefficient of slip λ and the tangential velocity. The coefficient of slip provides a measure of how much the cells adhere to the wall of the duct, so when $\lambda = 0$ the tumour surface is flat and the movement of the cells one-dimensional in z (i.e. plug flow).

2.2. Non-dimensionalisation

Denoting dimensionless variables by carets and using the rate of cell proliferation to set the timescale, we introduce the following rescalings:

$$t = \frac{\hat{t}}{A}, \qquad c = c_I \hat{c}, \qquad n = \hat{n}, \qquad r = h\hat{r},$$
$$p = p_I \hat{p}, \qquad z = h\hat{z}, \qquad u = hA\hat{u}, \qquad v = hA\hat{v},$$

where h, p_I and c_I denote typical length, pressure and concentration scales (based on the initial conditions). Substituting into our system gives the following dimensionless equations

$$\frac{\partial \hat{n}}{\partial \hat{t}} = -\hat{\nabla} \cdot (\hat{n}\hat{\mathbf{v}}) + (\hat{k_m}(\hat{c}) - \hat{k_d}(\hat{c}))\hat{n} + \hat{D}_n \hat{\nabla}^2 \hat{n}, \tag{11}$$

$$\hat{\nabla} \cdot \hat{\mathbf{v}} = \hat{k_m}(\hat{c})\hat{n}, \tag{12}$$

$$\frac{\partial \hat{p}}{\partial \hat{r}} = \hat{\mu}\left(\hat{\nabla}^2 \hat{u} - \frac{\hat{u}}{\hat{r}^2} + \frac{1}{3}\frac{\partial}{\partial \hat{r}}(\hat{\nabla} \cdot \hat{\mathbf{v}})\right) + \frac{4}{3}\frac{\partial \hat{\mu}}{\partial \hat{r}}\left(\frac{\partial \hat{u}}{\partial \hat{r}} - \frac{1}{2}\left(\frac{\hat{u}}{\hat{r}} + \frac{\partial \hat{v}}{\partial \hat{z}}\right)\right) + \frac{\partial \hat{\mu}}{\partial \hat{z}}\left(\frac{\partial \hat{u}}{\partial \hat{z}} + \frac{\partial \hat{v}}{\partial \hat{r}}\right), \tag{13}$$

$$\frac{\partial \hat{p}}{\partial \hat{z}} = \hat{\mu}\left(\hat{\nabla}^2 \hat{v} + \frac{1}{3}\frac{\partial}{\partial \hat{z}}(\hat{\nabla} \cdot \hat{\mathbf{v}})\right) + \frac{4}{3}\frac{\partial \hat{\mu}}{\partial \hat{z}}\left(\frac{\partial \hat{v}}{\partial \hat{z}} - \frac{1}{2}\left(\frac{\hat{u}}{\hat{r}} + \frac{\partial \hat{u}}{\partial \hat{r}}\right)\right) + \frac{\partial \hat{\mu}}{\partial \hat{r}}\left(\frac{\partial \hat{u}}{\partial \hat{z}} + \frac{\partial \hat{v}}{\partial \hat{r}}\right), \tag{14}$$

$$\hat{\nabla}^2 \hat{c} = \hat{\beta}\hat{k_m}(\hat{c})\hat{n}. \tag{15}$$

In (15) we have adopted the simpler (quasi-steady) form for the nutrient concentration as we find from the non-dimensionalisation that the left hand side of equation (5) is negligible in comparison to the right hand side. This implies that diffusion, rather than convection is the dominant mechanism for the redistribution of nutrient within the tumour (see [13] for details). The dimensionless parameters are

$$\hat{k_m}(\hat{c}) = c, \quad \hat{k_d}(\hat{c}) = \hat{B}\,(1 - \sigma c)\,, \quad \hat{B} = \frac{B}{A}, \quad \hat{D}_n = \frac{D_n}{Ah^2},$$
$$\hat{\beta} = \frac{\beta A h^2}{D}, \quad \hat{\mu} = \frac{\mu A}{p_I}, \quad \hat{\lambda} = \frac{\lambda A h}{p_I}.$$

The boundary conditions for this dimensionless system are given by

$$\begin{aligned}
&\text{on } \hat{z}=0 \quad \frac{\partial \hat{n}}{\partial \hat{z}}=0, \quad \frac{\partial \hat{p}}{\partial \hat{z}}=0, \quad \frac{\partial \hat{u}}{\partial \hat{z}}=0, \quad \hat{v}=0, \quad \frac{\partial \hat{c}}{\partial \hat{z}}=0,\\
&\text{as } \hat{z}\to\infty \ \hat{n}=0, \quad \hat{u}=0, \quad \frac{\partial \hat{v}}{\partial \hat{z}}=0, \quad \hat{c}=1,\\
&\text{on } \hat{r}=0 \quad \frac{\partial \hat{n}}{\partial \hat{r}}=0, \quad \frac{\partial \hat{p}}{\partial \hat{r}}=0, \quad \hat{u}=0, \quad \frac{\partial \hat{v}}{\partial \hat{r}}=0, \quad \frac{\partial \hat{c}}{\partial \hat{r}}=0,\\
&\text{on } \hat{r}=1 \quad \frac{\partial \hat{n}}{\partial \hat{r}}=0, \quad \hat{u}=0, \quad \hat{\mu}\frac{\partial \hat{v}}{\partial \hat{r}}=-\hat{\lambda}\hat{v}, \quad \hat{c}=1,
\end{aligned} \tag{16}$$

and initial conditions by (9).

In general, when the viscosity is non-constant our model comprises a system of five coupled equations (11)–(15) which is non-trivial to solve. However, if we assume that the viscosity has the same value inside and outside of the tumour, the pressure, velocity and nutrient concentration can be found in terms of the tumour cell concentration only (see the following section) and hence the system simplifies significantly. We therefore focus on this case in the following section where numerical solutions are presented. We then adopt a thin film approximation to construct asymptotic solutions to the full system.

2.3. Numerical method and results for uniform viscosity ($\hat{\mu}(1)=\hat{\mu}(0)=1$)

2.3.1. Numerical method

We take the viscosity in and outside the tumour to be uniform ($\hat{\mu}=1$ for all $\hat{n}$), so the tumour and surrounding fluid have similar material properties. Henceforth we drop the carets for brevity. Taking the divergence of (13), (14) and the Laplacian of (12) we deduce that the pressure satisfies

$$\nabla^2 p = \frac{4}{3}\nabla^2\left(k_m(c)n\right). \tag{17}$$

Moreover, using (13) and (14) we find that the velocity satisfies

$$\nabla^2 \mathbf{v} = \nabla p - \frac{1}{3}\nabla\left(k_m(c)n\right). \tag{18}$$

As the order of the system (equations (11), (15)-(18)) has been increased by one, we need additional boundary conditions for the pressure. On the truncated domain $z=L$ the pressure $p=0$; an additional condition on the duct wall can be deduced in the following manner. With $\mu=1$, equation (13) states

$$\frac{\partial p}{\partial r} = \nabla^2 u - \frac{u}{r^2} + \frac{1}{3}\frac{\partial}{\partial r}\left(k_m(c)n\right). \tag{19}$$

Differentiating (12) with respect to r, substituting into (19) and imposing the conditions for v and n on the rigid boundary (where $\partial v/\partial r=-\lambda v$, $\partial n/\partial r=0$) we deduce that

$$\frac{\partial p}{\partial r} = \lambda\frac{\partial v}{\partial z} + \frac{4}{3}n\frac{\partial}{\partial r}(k_m(c)) \qquad \text{on } r=1. \tag{20}$$

We may therefore solve equations (11), (15)-(18) in turn, using a predictor-corrector method [19] with NAG routing D03EBF (which calculates the solution to a system of simultaneous equations derived from approximating the Laplacian using a central difference scheme), with boundary conditions on $z = 0$, $r = 0$ and $r = 1$ given by (16), (20) and those on $z = L$ by

$$\text{on } z = L \qquad n = 0, \quad p = 0. \tag{21}$$

The truncated domain $L = 200$ and suitably smoothed initial conditions (cf. (9)) read

$$n = \frac{1}{2}(1 - \tanh(100(z - 1))),$$

so that initially, the tumour front is taken to be a relatively sharp interface.

2.3.2. Numerical results

Using parameter estimates based on experimental values summarised in [22], we employ the following values for the dimensionless quantities β, σ and B (unless otherwise stated)

$$B = 1, \quad \sigma = 0.9, \quad \beta = 0.1, \quad \lambda = 5, \quad D_n = D_m = D_\rho = 10^{-5}.$$

Figure 1(a) shows a surface plot of the live cell concentration, in which the region where $n \approx 0.9$ defines the tumour (the dead cell concentration $m \approx 0.1$ in this region). The nutrient is diffusing in from the duct wall $r = 1$ (see Figure 4(a) for concentration profile) and from the tumour surface (n is greatest in these places). As the duct wall is rigid and of fixed radius, and the rate at which cells consume nutrient is low ($\beta = 0.1$), all cells receive adequate levels of nutrient and cell death within the tumour is limited. Consequently, the live cell concentration falls to about 0.9 in the centre of the duct and remains at this level. If we increase the nutrient consumption rate (Figure 4(b)) the proportion of live tumour cells in the centre decreases (Figure 1(b)). Increasing β corresponds to an increase in either the

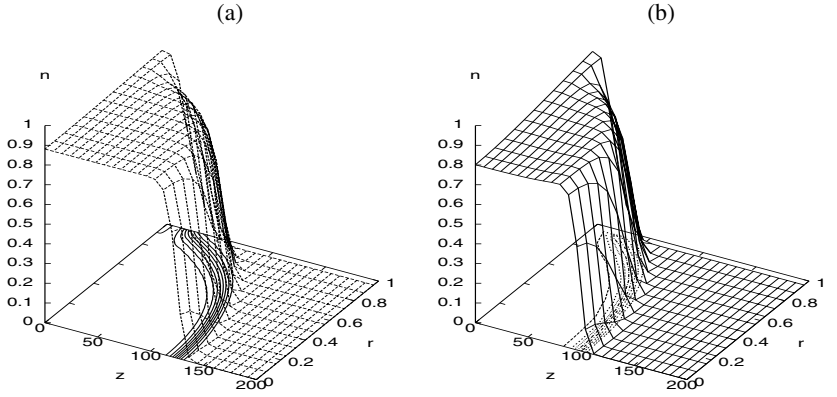

Fig. 1. Surface and contour plots of the tumour cell concentration at $t = 4$ with (a) $\beta = 0.1$ and (b) $\beta = 0.5$.

consumption rate or the diameter of the duct (the non-dimensionalisation in Section 2.1 gives $\beta \propto h^2$). It follows that the larger the duct radius, the more nutrient will be consumed and the more cells will die in the centre of the duct (compare Figures 1(a) and (b)). This explains, in part, why a necrotic core is seen in high grade DCIS (where the duct is large and distended) and why it is absent in low grade DCIS. It should be noted that as the diffusion terms are very small, the only effect of their inclusion is to smear out the front over the range $z = O(\sqrt{D_n/k_m(c)})$ (the relevant asymptotics are studied in detail in [16]), and the values of the diffusivities do not therefore affect the quantitative behaviour except by smearing out the moving boundary. Hence, the system is not in fact sensitive to the values of the diffusion coefficients.

Figure 2(a) shows the surface plot of the pressure that corresponds to Figure 1(a). The pressure is greatest on the duct wall at the centre of the tumour, i.e. at $z = 0$, $r = 1$, and we observe in Figure 2(b) that the pressure there increases rapidly with time. These factors are due to cellular proliferation creating a net force on the cells which increases with distance from the surface. Over time and as more cells are produced, cells near the centre have to push against an increasing amount of cellular material in order to create space for the new cells. We remark that the pressure on the duct wall is greater than that at the centre. This is because the wall acts as a source of nutrient and hence there is greater net cell proliferation there. Figure 2(b) shows how the pressure at the centre evolves for different choices of the nutrient consumption rate β. As one might expect, the pressure is greatest when no nutrient is consumed ($\beta = 0$) and most cells are proliferating with minimal cell death.

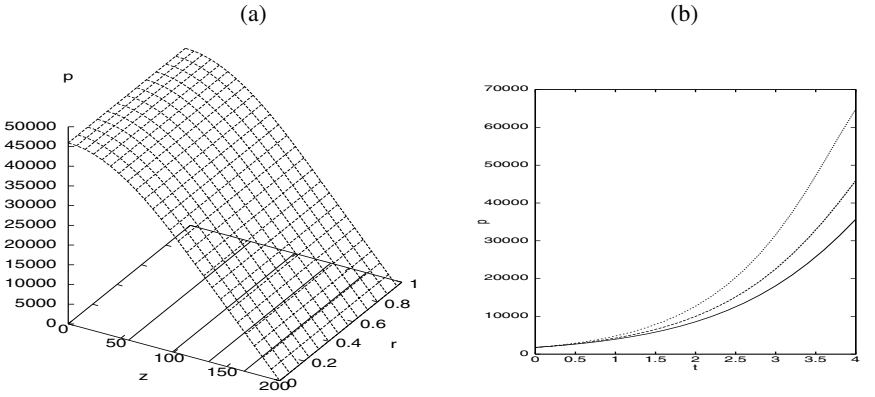

Fig. 2. (a) Surface and contour plot of the pressure at $t = 4$ when $\beta = 0.1$. (b) Series of plots showing how the evolution of the pressure at the centre of the duct changes when β varies ($\beta = 0.5$ (solid line), $\beta = 0.1$ (dashed line), $\beta = 0$ (dotted line)).

Figures 3(a) and (b) show the radial and axial velocities that correspond to Figure 1(a). The tumour cells are moving slowly in the radial direction towards the centre as the new cells find it preferable to push against other cells, rather than the rigid wall. On the tumour surface, proliferating cells migrate slowly outwards in the radial direction as they encounter no resistance. At the centre, $z = 0$, cells

are stationary but as we approach the surface, increasing numbers of new cells are pushing out those outside them, resulting in the axial velocity increasing approximately linearly with respect to z. The velocity is approximately constant in the surrounding region as there are no cells there to divide. As expected, cells near the duct wall move more slowly than those in the centre of the duct because they adhere to the wall. It should be noted that the magnitude of the axial velocity is much greater than the radial velocity as cells move preferentially along the duct, following the path of least resistance.

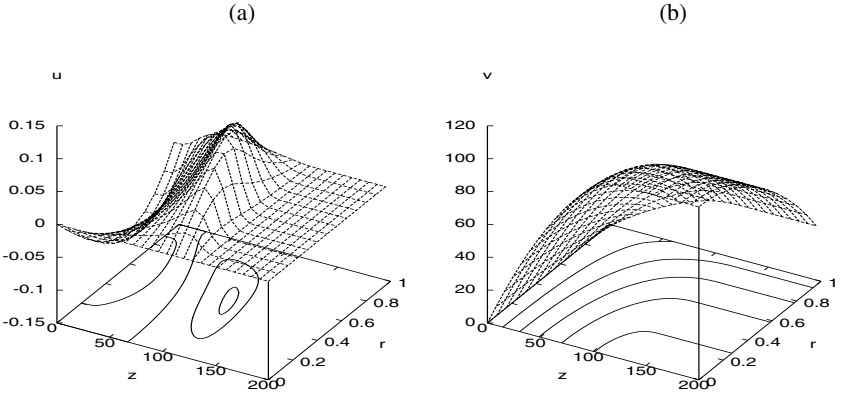

Fig. 3. Surface and contour plots of (a) the radial velocity, u and (b) the axial velocity, v at $t = 4$.

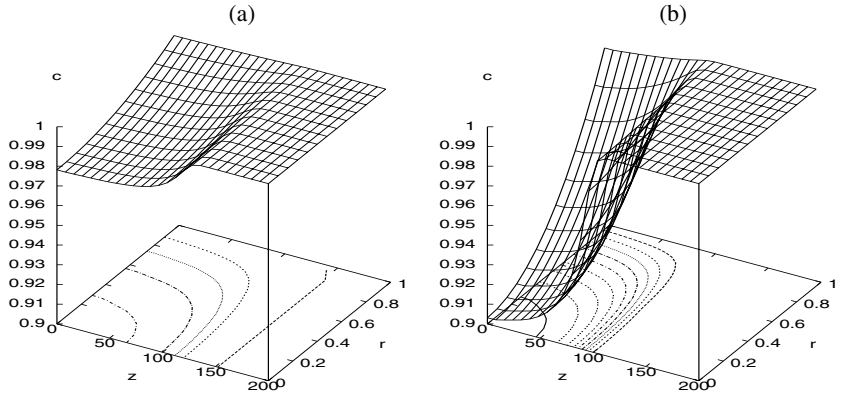

Fig. 4. Surface and contour plot of the nutrient concentration at $t = 4$ with (a) $\beta = 0.1$ and (b) $\beta = 0.5$.

Figures 5 and 6 show how the shape and evolution of the tumour surface (specified for definiteness as the contour $n = 0.5$) change when the parameters β and λ are varied. Referring to Figure 5, we note that as β increases and hence more nutrient is consumed, cells furthest from nutrient sources die more rapidly. Fewer cells then proliferate and the tumour is smaller.

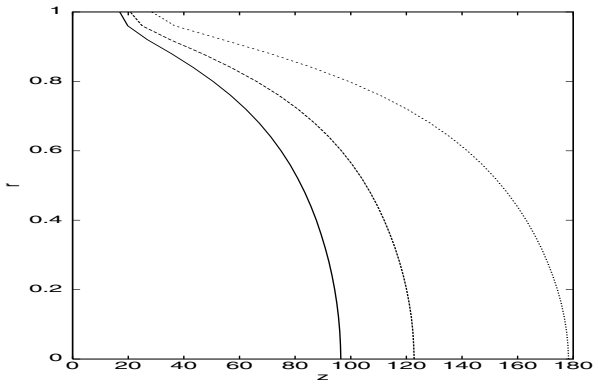

Fig. 5. Comparison of the tumour surface location for the nutrient-limited model ($\beta = 0.5$ (solid line), $\beta = 0.1$ (dashed line)) and the nutrient rich case ($\beta = 0$ (dotted line)) at $t = 4$, (the contours have $n = 0.5$).

Figures 6(a) and (b) show the effect on the tumour surface of varying the extent to which cells adhere to the duct wall (note the difference in domain sizes in (a) and (b)). For moderate values of λ ($\lambda = 1$) the cells can slip fairly readily along the duct wall and the tumour surface is reasonably flat, whereas for larger values of λ ($\lambda = 5$), the cells have a greater tendency to stick to the wall and the surface becomes more elongated.

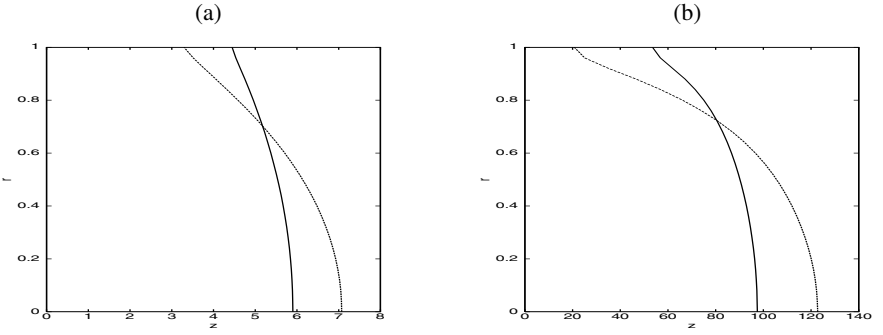

Fig. 6. Tumour boundary at (a) $t = 1$ and (b) $t = 4$. The contours are $n = 0.5$ with $\lambda = 1$ (solid line) and $\lambda = 5$ (dashed line).

To summarise, in this section we have used numerical methods to show how the tumour grows inside a rigid walled cylinder when the viscosity is uniform across the tumour and the surrounding fluid. If the doubling time of the tumour cells is of $O(14\text{hours})$ (cf. [22]), it follows that $A \approx 10^{-5}s^{-1}$. The dimensional time is then approximately the dimensionless time in days. Of course, the model only considers the case when the cells are at a fixed distance from the nutrient source (as the wall is rigid). The effect of nutrient limitations will become more pronounced when the wall is compliant. In the following section we use analytical methods to examine cases for which the viscosity is not uniform and the aspect ratio of the tumour is

small. We also assume that the cells are growing in a nutrient-rich environment, justifying this approximation by making reference to Figures 4(a) and (b) which show that $c \approx 1$ throughout the tumour. Since cells typically become hypoxic when they are further than 0.2mm from a nutrient source [20], this approximation will be valid for normal ducts which are assumed rigid and are 0.2-0.4mm in diameter.

3. Sharp interface limit $D_n = 0$

When $D_n = 0$, the tumour surface is a sharp interface which we denote by $z = s(r, t)$. We assume nutrient-rich conditions with no cell death ($k_d = 0$) and no consumption of nutrient ($\beta = 0$). Under these assumptions, our dimensionless system (with $c = 1$ and μ taken to be piecewise constant) becomes

$$\frac{\partial n}{\partial t} + \nabla \cdot (n\mathbf{v}) = k_m(1)n, \tag{22}$$

$$\nabla \cdot \mathbf{v} = k_m(1)n, \tag{23}$$

$$\nabla p = \mu \left(\nabla^2 \mathbf{v} + \frac{1}{3} \nabla(\nabla \cdot \mathbf{v}) \right). \tag{24}$$

The boundary conditions for n, u, v and p are given by (16) and the initial conditions by (9), so that the tumour initially consists of live cells only ($n = 1$, $\rho = m = 0$) and the exterior consists solely of extracellular fluid ($\rho = 1$, $n = m = 0$).

Since the tumour surface is now a sharp interface, we must also impose continuity of the stress and velocity components there. The superscript notation is introduced to distinguish between the two sides of the tumour boundary, with, for example, u^+ and u^- representing respectively the radial velocity to the right and left of the interface and $[u]^+_- = u^+ - u^-$. Using this notation we deduce that the normal and tangential components of the stress tensor and the radial and axial components of the velocity will be continuous if

$$[u]^+_- = [v]^+_- = 0, \tag{25}$$

$$[p - 2\mu(e_{ij} n_i n_j - e_{ii}/3)]^+_- = 0, \tag{26}$$

$$[\mu e_{ij} t_i n_j]^+_- = 0. \tag{27}$$

In (26)-(27) the normal and tangential unit vectors are given by

$$\mathbf{n} = \frac{(-\partial s/\partial r, 1)}{(1 + (\partial s/\partial r)^2)^{1/2}}, \qquad \mathbf{t} = \frac{(1, \partial s/\partial r)}{(1 + (\partial s/\partial r)^2)^{1/2}}. \tag{28}$$

The evolution of the tumour surface is determined from the kinematic condition on the interface which states that the fluid particles on the surface of the tumour remain there, so

$$\frac{\partial s}{\partial t} = v - u \frac{\partial s}{\partial r}. \tag{29}$$

We focus on this limit for the analysis in the remainder of this paper.

4. The slender approximation

4.1. Asymptotic analysis

Recent 3D histo-pathology of DCIS [11] shows that the tumour is typically much longer in the axial direction than in the radial direction. Indeed, on the basis of our clinical experience (J.C.E. Underwood), DCIS commonly extends a distance of 20mm or more along a duct compared with an average diameter of 0.7mm. This is consistent with the numerical simulations in Section 2.3.2 which show that for large times, the tumour front becomes much longer in the axial direction than in the radial direction. The model can therefore be simplified by adopting a thin-film approximation to construct asymptotic solutions to examine cases for which the aspect ratio of the tumour is small. Defining $\epsilon \ll 1$ as the ratio of the radial to the axial distance, the variables can be scaled as follows:

$$z = \epsilon^{-1} z^*, \quad u = u^*, \quad v = \epsilon^{-1} v^*, \quad r = r^*,$$
$$p = \epsilon^{-2} p^*, \quad n = n^*, \quad t = k_m(1)^{-1} \ln(\epsilon^{-1}) + t^*.$$

Substituting these new variables into equations (22)–(24) and equating to zero coefficients of $O(\epsilon^n)$ we obtain the following equations:

$$O(\epsilon^{-2}): \qquad \frac{\partial p^*}{\partial r^*} = 0, \tag{30}$$

$$O(\epsilon^{-1}): \qquad \frac{\partial p^*}{\partial z^*} = \frac{\mu}{r^*} \frac{\partial}{\partial r^*} \left(r^* \frac{\partial v^*}{\partial r^*} \right), \tag{31}$$

$$O(1): \qquad \frac{1}{r^*} \frac{\partial}{\partial r^*} (r^* u^*) + \frac{\partial v^*}{\partial z^*} = k_m(1) n^*. \tag{32}$$

In (32) n^* is taken to be a step function ($n^* = 1$ in the tumour and $n^* = 0$ outside) and $k_m(1)$ is the constant proliferation rate.

We divide the tumour into three regions (see Figure 7): (1) a region in which the duct is fully occupied by the tumour, (2) a region containing tumour cells and the surrounding material, in which the tumour loses contact with the duct wall, (3) a tumour-free region containing surrounding material only. We decompose region (2) into subregions containing either tumour cells or surrounding material. These subregions are separated by the interface $z^* = s(r^*, t^*)$ which marks the tumour boundary. The position at which the tumour leaves the wall and the position of the tip move as the tumour grows and are denoted by $z^* = S_T(t^*)$ and $z^* = S_S(t^*)$ respectively.

We solve equations (30)-(32) in regions (1)-(3) using the following conditions for u^*, v^*, and p^* on $r^* = 0$, $r^* = 1$, $z^* = 0$ and $z^* \to \infty$ in the appropriate

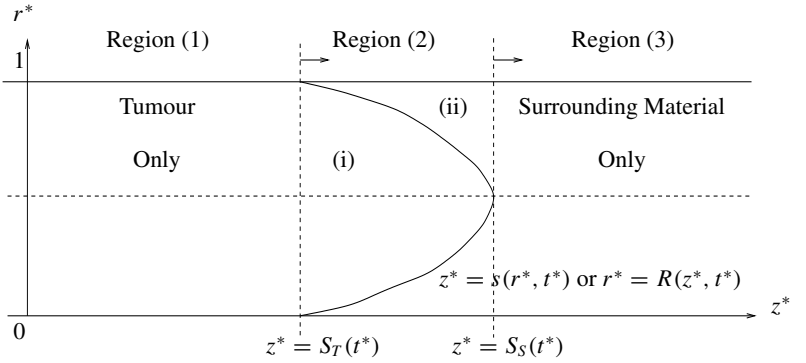

Fig. 7. A schematic showing how the duct is decomposed into three separate regions.

regions.

$$\begin{aligned}
&\text{on } r^* = 0 \quad u^* = 0, \quad \frac{\partial v^*}{\partial r^*} = 0, \quad \frac{\partial p^*}{\partial r^*} = 0,\\
&\text{on } r^* = 1 \quad u^* = 0, \quad \mu\frac{\partial v^*}{\partial r^*} = -\lambda v^*,\\
&\text{on } z^* = 0 \quad \frac{\partial u^*}{\partial z^*} = 0, \quad v^* = 0, \quad \frac{\partial p^*}{\partial z^*} = 0,\\
&\text{as } z^* \to \infty \; u^* = 0, \quad \frac{\partial v^*}{\partial z^*} = 0.
\end{aligned} \tag{33}$$

In region (2) we impose the continuity conditions (25)-(27) on the surface $r^* = R(z^*, t^*)$ (or $z^* = s(r^*, t^*)$). On rescaling these conditions reduce to give:

$$[u^*]^+_- = 0, \quad [v^*]^+_- = 0, \quad [p^*]^+_- = 0, \quad [\mu\partial v^*/\partial r^*]^+_- = 0. \tag{34}$$

By solving (30)-(32) we obtain expressions for p^*, u^* and v^* in each of the three regions; these are stated in turn below.

– **Region (1): Tumour only** ($\mu = \mu(1), 0 < z^* < S_T(t^*)$)
In this region the tumour occupies the entire duct (i.e. $n^* = 1$ and $R(z^*, t^*) = 1$). Imposing conditions for u^*, v^* and p^* on $r^* = 0$, $r^* = 1$ and $z^* = 0$ given by (33) gives

$$\frac{\partial^2 p^*}{\partial z^{*2}} = -\frac{8k_m(1)\lambda\mu(1)}{\lambda + 4\mu(1)}, \tag{35}$$

$$v^* = \frac{1}{4\mu(1)}\frac{\partial p^*}{\partial z^*}\left(r^{*2} - \frac{2\mu(1)}{\lambda} - 1\right), \tag{36}$$

$$u^* = \frac{k_m(1)r^*}{2} - \frac{r^*}{16\mu(1)}\frac{\partial^2 p^*}{\partial z^{*2}}\left(r^{*2} - \frac{4\mu(1)}{\lambda} - 2\right). \tag{37}$$

– **Region (2): Tumour and surrounding material subregions** ($S_T(t^*) < z^* < S_S(t^*)$)

In this region the tumour leaves the duct wall. We impose conditions for u^* and v^* on $r^* = 0$ in subregion (i) ($r^* < R(z^*, t^*)$) and conditions on $r^* = 1$ in subregion (ii) ($r^* > R(z^*, t^*)$) given by (33). We then impose the continuity conditions given by (34) on the tumour boundary $r^* = R(z^*, t^*)$. In this way we obtain the following expressions for p^*, v^* and u^*:

– **Subregion (i): Tumour** ($\mu = \mu(1)$)

$$p^* = p^*(z^*, t^*), \tag{38}$$

$$v^* = \frac{1}{4\mu(1)} \frac{\partial p^*}{\partial z^*} \left(r^{*2} - \frac{2\mu(1)}{\lambda} - R^2 - \frac{\mu(1)}{\mu(0)}(1 - R^2) \right), \tag{39}$$

$$u^* = \frac{k_m(1) r^*}{2} - \frac{R r^*}{4\mu(1)} \frac{\partial p^*}{\partial z^*} \frac{\partial R}{\partial z^*} \left(\frac{\mu(1)}{\mu(0)} - 1 \right) - \frac{r^*}{16\mu(1)} \frac{\partial^2 p^*}{\partial z^{*2}} \left(r^{*2} - \frac{4\mu(1)}{\lambda} - 2R^2 - 2\frac{\mu(1)}{\mu(0)} \left(1 - R^2 \right) \right). \tag{40}$$

– **Subregion (ii): Surroundings** ($\mu = \mu(0)$)

$$p^* = p^*(z^*, t^*), \tag{41}$$

$$v^* = \frac{1}{4\mu(0)} \frac{\partial p^*}{\partial z^*} \left(r^{*2} - \frac{2\mu(0)}{\lambda} - 1 \right), \tag{42}$$

$$u^* = -\frac{r^*}{16\mu(0)} \frac{\partial^2 p^*}{\partial z^{*2}} \left(r^{*2} - \frac{4\mu(0)}{\lambda} - 2 + \frac{1}{r^{*2}} \left(1 + \frac{4\mu(0)}{\lambda} \right) \right). \tag{43}$$

Continuity of u^* on $r^* = R(z^*, t^*)$ leads to the following partial differential equation for $p^*(z^*, t^*)$:

$$\frac{\partial}{\partial z^*} \left[\frac{\partial p^*}{\partial z^*} \left\{ R^4 \left(\frac{1}{\mu(1)} - \frac{1}{\mu(0)} \right) + \left(\frac{1}{\mu(0)} + \frac{4}{\lambda} \right) \right\} \right] = -8 k_m(1) R^2. \tag{44}$$

To determine the evolution of the tumour surface $r^* = R(z^*, t^*)$, we impose the kinematic condition on the interface ($\partial R / \partial t^* = u^* - v^* \partial R / \partial z^*$). We then get

$$\frac{\partial}{\partial t^*}(R^2) = k_m(1) R^2 - \frac{1}{4} \frac{\partial}{\partial z^*} \left[R^2 \frac{\partial p^*}{\partial z^*} \left\{ R^2 \left(\frac{1}{\mu(0)} - \frac{1}{2\mu(1)} \right) - \left(\frac{1}{\mu(0)} + \frac{2}{\lambda} \right) \right\} \right]. \tag{45}$$

Equations (44) and (45) for $R(z^*, t^*)$ and $p^*(z^*, t^*)$ in region (2) are solved subject to initial and boundary conditions detailed below. We note that p^* and R are continuous across $z^* = S_T(t^*)$ and $z^* = S_S(t^*)$.

– **Region (3): Surrounding material only** ($\mu = \mu(0)$, $S_S(t^*) < z^* < \infty$)
In this region, the surrounding material occupies the duct so $R(z^*, t^*) = 0$. As in region (1), we impose boundary conditions (33) for u^*, v^* and p^* on $r^* = 0$, $r^* = 1$ and as $z^* \to \infty$.

$$\frac{\partial^2 p^*}{\partial z^{*2}} = 0, \tag{46}$$

$$v^* = \frac{1}{4\mu(0)} \frac{\partial p^*}{\partial z^*} \left(r^{*2} - \frac{2\mu(0)}{\lambda} - 1 \right), \tag{47}$$

$$u^* = 0. \tag{48}$$

We remark that the position of the tumour surface in regions (1) and (3) is known. It remains to determine p^* in each of the three regions (i.e. equations (35), (44) and (46)) and R in region (2) (equation (45)). Boundary conditions on $S_T(t^*)$ and $S_S(t^*)$ are determined below and u^*, v^*, p^* and R are all continuous across these points.

We notice that p^* only appears as its derivative with respect to z^* so defining $P = \partial p^*/\partial z^*$ and letting $A = R^2$ we obtain the following expressions for P and A is each region.

$$P = -\frac{8k_m(1)\lambda\mu(1)}{\lambda + 4\mu(1)} z^*, \qquad A = 1, \tag{49}$$

in region (1). In region (2) we have

$$8k_m(1)A = \frac{\partial}{\partial z^*} \left[P \left\{ A^2 \left(\frac{1}{\mu(0)} - \frac{1}{\mu(1)} \right) - \left(\frac{1}{\mu(0)} + \frac{4}{\lambda} \right) \right\} \right], \tag{50}$$

$$\frac{\partial A}{\partial t^*} = k_m(1)A - \frac{1}{4} \frac{\partial}{\partial z^*} \left[AP \left\{ \left(\frac{1}{\mu(0)} - \frac{1}{2\mu(1)} \right) A - \left(\frac{1}{\mu(0)} + \frac{2}{\lambda} \right) \right\} \right], \tag{51}$$

and in region (3) we get

$$\frac{\partial P}{\partial z^*} = 0, \qquad A = 0, \tag{52}$$

with $P = 0$ on $z^* = 0$ and $A \to 0$ as $z^* \to +\infty$. Using equations (49), (51) and (52) and integrating over the length of the duct we deduce

$$\frac{d}{dt^*} \int_0^\infty A dz^* = k_m(1) \int_0^\infty A dz^* \Rightarrow \int_0^\infty A dz^* = A_0 \exp\left(k_m(1)t^*\right) \tag{53}$$

where $A_0 = \int_0^\infty A(z^*, 0) dz^*$ represents the initial volume of the tumour. Using (53) we find that the tumour volume is increasing exponentially with time and that its growth rate depends on the proliferation rate $k_m(1)$ alone. This is to be expected as growth occurs through cell division only and there is no degradation of dead cells.

The position at which the tumour leaves the duct wall and the locus of the tumour tip are determined as follows. Substituting for u^* and v^* from (35)-(37) into the kinematic condition (29), we deduce that on $z^* = S_T(t^*)$, where $r^* = 1$ and $u^* = 0$,

$$\frac{dS_T}{dt^*} = \frac{4k_m(1)\mu(1)}{\lambda + 4\mu(1)} S_T. \tag{54}$$

Integrating equation (54) we deduce that the point $z^* = S_T(t^*)$ at which the tumour loses contact with the rigid duct wall satisfies

$$S_T(t^*) = S_T(0) \exp\left(\frac{k_m(1)t^*}{\frac{\lambda}{4\mu(1)} + 1}\right), \tag{55}$$

where $S_T(0)$ is the initial position at which the tumour leaves the wall. Comparing (53) and (55) and noting that λ and $\mu(1)$ are positive parameters, we deduce that the contact point moves at a slower rate than that at which the tumour volume is increasing. This is because the cells adhere to the duct wall.

We proceed in a similar manner as above to determine the position of the tumour tip. Substituting for u^* and v^* from (47) and (48), we deduce that on $z^* = S_S(t^*)$, where $r^* = 0$ and $A = 0$,

$$\frac{dS_S}{dt^*} = -\frac{1}{4}\left(\frac{1}{\mu(0)} + \frac{2}{\lambda}\right) P_{z^*=S_S(t^*)}, \tag{56}$$

Integrating equation (50) over the region $S_T(t^*) < z^* < S_S(t^*)$, we deduce that

$$\left(\frac{1}{\mu(0)} + \frac{4}{\lambda}\right) P_{z^*=S_S} = \left(\frac{1}{\mu(1)} + \frac{4}{\lambda}\right) P_{z^*=S_T} - 8k_m(1) \int_{S_T}^{S_S} A dz^*.$$

Using equation (49) to evaluate $P_{z^*=S_T}$, noting that $A = 1$ for $0 < z^* < S_T(t^*)$ and $A = 0$ for $S_S(t^*) < z^*$, and using equation (53), we deduce that

$$P_{z^*=S_S} = -\frac{8k_m(1)\lambda\mu(0)}{\lambda + 4\mu(0)} \int_0^\infty A dz^* = -\frac{8k_m(1)\lambda\mu(0)}{\lambda + 4\mu(0)} A_0 \exp\left(k_m(1)t^*\right),$$

and hence that

$$S_S(t) = S_S(0) + 2A_0 \frac{\lambda + 2\mu(0)}{\lambda + 4\mu(0)} \left(\exp\left(k_m(1)t^*\right) - 1\right), \tag{57}$$

where $S_S(0)$ is the initial tip position of the tumour. Thus the tip moves out at the same rate as the tumour increases in volume. This is to be expected since for the nutrient-rich model we are considering cells which have no growth constraints placed upon them.

4.2. Numerical method and results

The position at which the tumour leaves the wall and the position of the tip of the tumour are known explicitly (see (55) and (57)) and P and A are known in regions (1) and (3). We solve (50) and (51) numerically to determine P and A in region (2) using the following boundary conditions on $z^* = S_T(t^*)$ and $z^* = S_S(t^*)$.

$$\text{on } z^* = S_T(t^*): \qquad P = -\frac{8k_m(1)\mu(1)\lambda}{(\lambda + 4\mu(1)))} S_T, \tag{58}$$

$$\text{on } z^* = S_S(t^*): \qquad A = 0, \tag{59}$$

To solve numerically we first fix the positions of the two moving boundaries $z^* = S_T(t^*)$ and $z^* = S_S(t^*)$ by mapping the domain $S_T \le z^* \le S_S$ onto a unit interval using the translation $z^* = (S_S(t^*) - S_T(t^*))\hat{z} + S_T(t^*)$. The initial conditions are then taken to be $A = 1 - \hat{z}^{10}$ so that the tumour almost completely occupies the diameter of the duct, just leaving the duct wall at the tumour front. The evolution of the two moving boundaries is determined from

$$\frac{dS_T}{dt^*} = -\frac{1}{2\lambda} P_{\hat{z}=0}, \qquad \frac{dS_S}{dt^*} = -\frac{1}{4}\left(\frac{1}{\mu(0)} + \frac{2}{\lambda}\right) P_{\hat{z}=1},$$

where $S_T(0) = 1$ and $S_S(0) = 2$. The results are shown for uniform and variable viscosity in the following sections.

4.2.1. Uniform viscosity ($\mu(1) = \mu(0) = 1$)

In practice we would expect the surrounding material to be less viscous than the tumour as it consists of extracellular fluid. However, we first consider the case when the viscosities of the tumour and surrounding material are equal so that comparisons can be made with the numerical simulations.

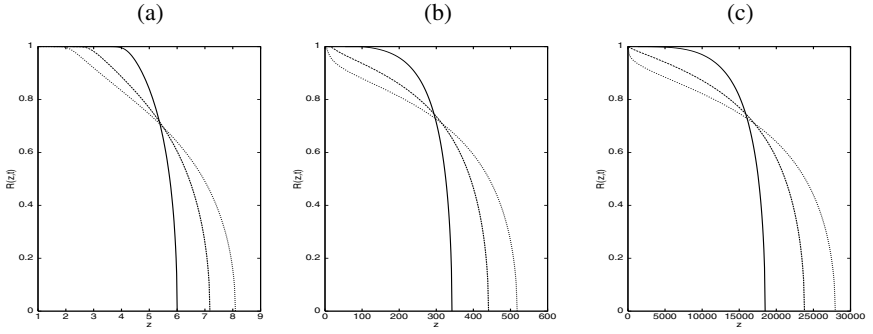

Fig. 8. Series of plots showing how, when $k_m(1) = 1$, the shape of the tumour surface $r^* = R(z^*, t^*)$ evolves for different choices of λ ($\lambda = 1$ (solid line), $\lambda = 5$ (dashed line) and $\lambda = 20$ (dotted line)). The surface is plotted at (a) $t^* = 1$, (b) $t^* = 5$ and (c) $t^* = 9$.

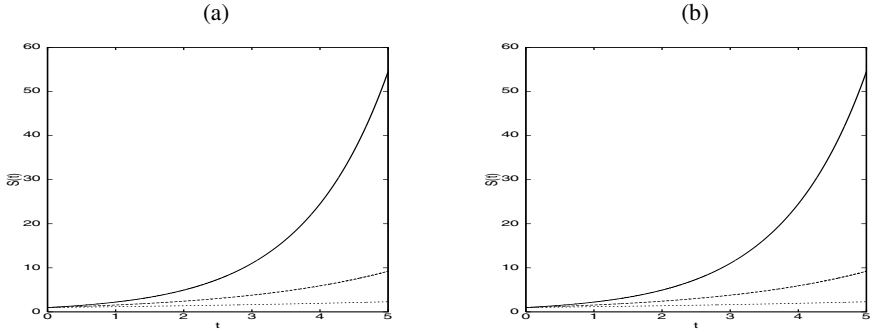

Fig. 9. Plots showing how when $k_m(1) = 1$, changes in λ ($\lambda = 1$ (solid line), $\lambda = 5$ (dashed line), $\lambda = 20$ (dotted line)) affect the evolution of (a) the tip of the tumour ($z^* = S_S(t^*)$ and (b) the point at which the tumour comes away from the duct wall ($z^* = S_T(t^*)$).

Figure 8 shows the effect on the tumour surface of varying λ, the degree to which the cells adhere to the duct wall. As λ decreases, the front becomes less elongated; when $\lambda = 0$ it is independent of z since the cells do not adhere to the wall and hence have no growth constraints. Figures 9(a) and (b) show how the loci $z^* = S_S(t^*)$ and $z^* = S_T(T^*)$ evolve for the values of λ used in Figure 8. As expected from equations (55) and (57), $S_T(t^*)$ decreases and $S_S(t^*)$ increases as λ increases.

A simple check of the numerical results is provided by equation (53). Calculating the volume of the tumour numerically we observe that it is conserved to within $\pm 10\%$. The discrepancy during the initial stages of growth is due to our approximation only being valid when the tumour is slender.

By definition, the slender approximation only holds when the tumour is much longer in the axial direction than it is in the radial direction. Comparison with the full problem will therefore only be applicable for large times. In Figure 10 we show that for late times, there is a good agreement between our asymptotic solution and the solution for the full problem.

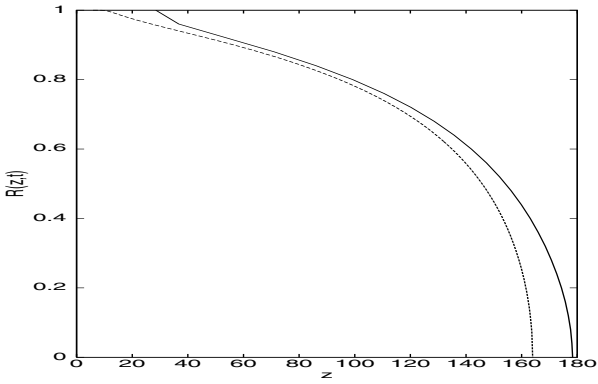

Fig. 10. Plots of the tumour surface $r^* = R(z^*, t^*)$ at $t^* = 4$ obtained by solving the full problem (solid line) and the slender approximation (dashed line).

4.2.2. Variable viscosity ($\mu(1) \neq \mu(0)$)

We now consider cases for which the tumour and surrounding fluid viscosities are no longer equal. We assume that the viscosity is piecewise constant (dependent upon the composition of the local material) and solve equations (50) and (51) subject to (58) and (59). For completeness, we consider cases for which the tumour is more and less viscous than the surrounding fluid, the more physical case arising when $\mu(1) > \mu(0)$ i.e. the tumour is more viscous than the extracellular fluid.

Figure 11 shows how the shape of the tumour boundary alters when $\mu(1) \neq \mu(0)$. When the surrounding medium is less viscous than the tumour ($\mu(1) > \mu(0)$), there is less resistance to the tumour's growth and the surface becomes elongated. Conversely, when $\mu(1) < \mu(0)$, there is more resistance to the tumour's growth and the surface is less elongated. The tumour grows at a constant rate, regardless of the viscosity ratio, its volume satisfying equation (53).

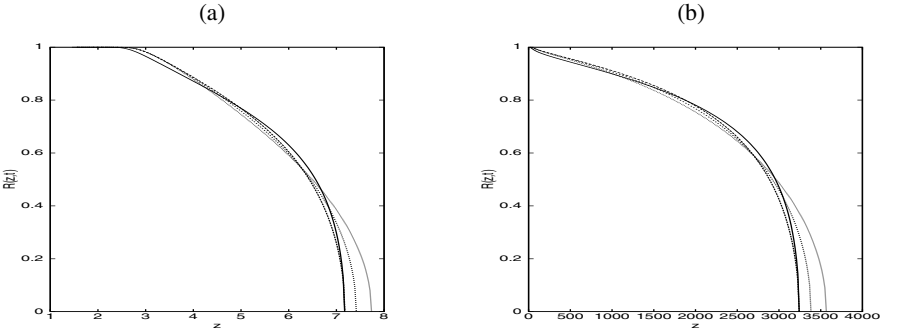

Fig. 11. Plots showing how, when $k_m(1) = 1$, the shape of the tumour surface at times (a) $t^* = 1$ and (b) $t^* = 7$ depends on the viscosities of the tumour and surrounding material ($\mu(1) = 0.75$, $\mu(0) = 1$ (solid line), $\mu(1) = 1$, $\mu(0) = 1$ (dashed line), $\mu(1) = 1$, $\mu(0) = 0.75$ (dotted line), $\mu(1) = 1$, $\mu(0) = 0.5$ (small dotted line)).

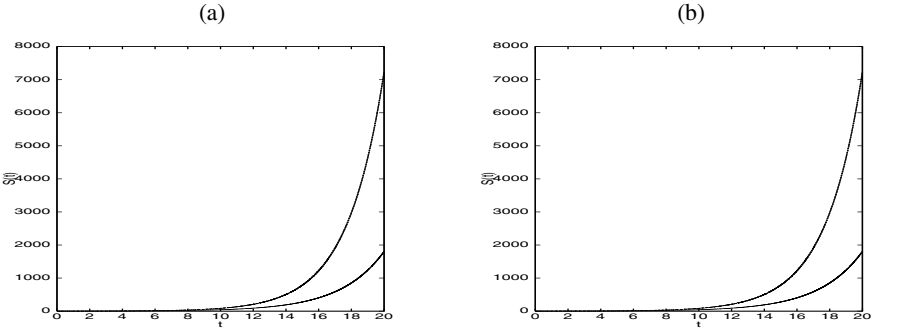

Fig. 12. Plots showing how the evolution of (a) the position of the tip of the tumour $z^* = S_S(t^*)$ and (b) the point at which the tumour leaves the duct wall $z^* = S_T(t^*)$ vary when the viscosities of the tumour and surrounding material change ($\mu(1) = 0.75$, $\mu(0) = 1$ (solid line), $\mu(1) = \mu(0) = 1$ (dashed line), $\mu(1) = 1$, $\mu(0) = 0.75$ (dotted line) and $\mu(1) = 1$, $\mu(0) = 0.5$ (small dotted line)). The results are for the simulations shown in Figure 11.

The positions of the tip of the tumour $S_S(t^*)$ and where the tumour leaves the duct wall $S_T(t^*)$ are shown in Figure 12. We know from equation (55) that the exponent of $S_T(t^*)$ is dependent upon the tumour viscosity and this is clearly shown in Figure 12(b). Figure 12(a) shows the position of the tip and we observe that, as given by equation (57), the exponent is the same for all viscosities, with the multiplying coefficient depending upon the surrounding viscosity.

4.3. Large time behaviour $t^* \to \infty$

The analysis and numerical simulations in Sections 4.1 and 4.2 show the tumour growing at an exponential rate. Redefining the axial co-ordinate z^* in the numerical simulations so that $\eta = z^* \exp(-k_m(1)t^*)$ and plotting the tumour surface $r^* = R(z^*, t^*)$ against η for large time, we observe self similar behaviour (see Figure 13(a)). Similarly, plotting the pressure gradient $P(z^*, t^*)$ against η shows

P growing exponentially with time, but plotting $\exp(-k_m(1)t^*)P(z^*, t^*)$ against η for large times gives a modified pressure gradient profile which is invariant with time (see Figure 13(b)). The example shown in Figure 13 is for when the viscosity is uniform. The self-similar behaviour is also seen when the viscosity is not uniform.

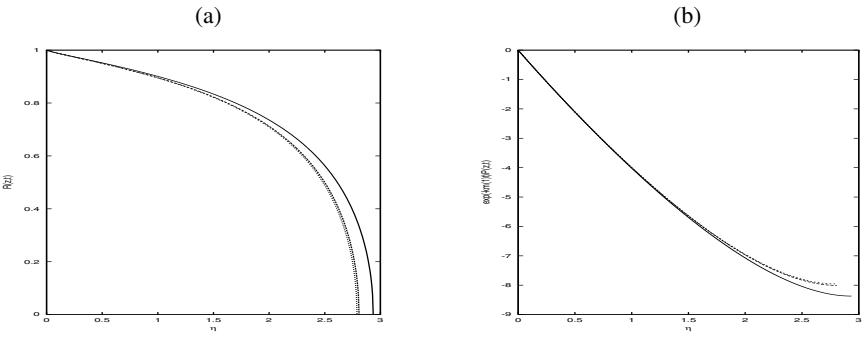

Fig. 13. (a) Tumour surface $R(z^*, t^*)$ and (b) pressure gradient $\exp(-k_m(1)t^*)P(z^*, t^*)$ profiles against η at $t^* = 20$ (solid line), $t^* = 24$ (dashed line) and $t^* = 28$ (dotted line) with $\lambda = 5$, $k_m(1) = 1$ and $\mu(1) = \mu(0) = 1$.

Guided by the results presented in Figure 13, we now investigate the large time behaviour of the tumour surface and pressure gradient by seeking similarity solutions to equations (50) and (51) of the form

$$P(z^*, t^*) \sim \exp(k_m(1)t^*)\hat{P}(\eta), \qquad A(z^*, t^*) \sim \hat{A}(\eta) \tag{60}$$

where $\eta = z^*/\exp(k_m(1)t^*)$. Substituting from (60) into equations (50) and (51) gives

$$\frac{d}{d\eta}\hat{P} = \frac{\lambda}{\mu(1)}\left(\frac{\mu(1)-\mu(0)}{\lambda+4\mu(0)}\right)\frac{d}{d\eta}(\hat{A}^2\hat{P}) - \frac{8k_m(1)\lambda\mu(0)}{\lambda+4\mu(0)}\hat{A}, \tag{61}$$

$$-k_m(1)\eta\frac{d}{d\eta}\hat{A} = k_m(1)\hat{A} - \frac{1}{4}\frac{d}{d\eta}\left[\hat{A}\hat{P}\left\{\hat{A}\left(\frac{1}{\mu(0)} - \frac{1}{2\mu(1)}\right) - \left(\frac{1}{\mu(0)} + \frac{2}{\lambda}\right)\right\}\right]. \tag{62}$$

Rearranging equation (62) and integrating once with respect to η, noting that $\hat{P} = 0$ on $\eta = 0$ (as $P(z^*, t) = 0$ on $z^* = 0$), we have

$$\hat{P} = \frac{4k_m(1)\eta}{\hat{A}\left(\frac{1}{\mu(0)} - \frac{1}{2\mu(1)}\right) - \left(\frac{1}{\mu(0)} + \frac{2}{\lambda}\right)}, \tag{63}$$

Substituting with equation (63) in (61) we obtain the following differential equation for $\hat{A}$:

$$8\hat{A} = \frac{d}{d\eta}\left[\frac{4\eta}{\hat{A}\left(\frac{1}{\mu(0)} - \frac{1}{2\mu(1)}\right) - \left(\frac{1}{\mu(0)} + \frac{2}{\lambda}\right)}\hat{A}^2\left(\frac{1}{\mu(0)} - \frac{1}{\mu(1)}\right)\right] - \frac{d}{d\eta}\left[\frac{4\eta}{\hat{A}\left(\frac{1}{\mu(0)} - \frac{1}{2\mu(1)}\right) - \left(\frac{1}{\mu(0)} + \frac{2}{\lambda}\right)}\left(\frac{1}{\mu(0)} + \frac{4}{\lambda}\right)\right], \tag{64}$$

which can be integrated to give an implicit solution for $\hat{A}$ of the form

$$\frac{\eta}{\eta_0} = \frac{(1-\hat{A})^{\frac{\lambda}{4\mu(1)}}\{2\mu(1)[\lambda + 2\mu(0)] + \lambda\hat{A}[\mu(0) - 2\mu(1)]\}}{\{4\mu(0) + \lambda[1-\hat{A}]\}^{\frac{(\lambda+4\mu(0))}{4\mu(1)}}}, \tag{65}$$

where η_0 is an integration constant and $0 \leq \hat{A} \leq 1$.

In Figure 14 we use equation (65) to plot $R(\eta) = \sqrt{\hat{A}(\eta)}$ for different choices of $\mu(0)$ and $\mu(1)$. The results, which are consistent with the $t^* = O(1)$ numerical simulations presented in Figure 11, show that the tumour surface becomes more elongated as $\mu(0)$ decreases and the resistance the surrounding fluid has on the tumour's expansion declines.

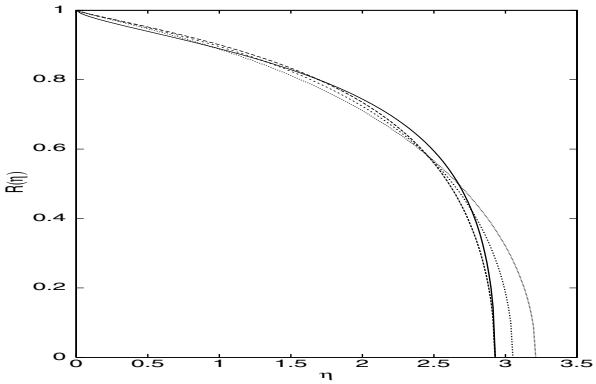

Fig. 14. Diagram showing how the large time behaviour of $R(\eta)$ varies with $\mu(1)$ and $\mu(0)$ when $\lambda = 5$, $\eta_0 = 1$: $\mu(1) = 0.75$ $\mu(0) = 1$ (solid line), $\mu(1) = 1$ $\mu(0) = 1$ (dashed line), $\mu(1) = 1$ $\mu(0) = 0.75$ (dotted line), $\mu(1) = 1$ $\mu(0) = 0.5$ (small dotted line).

Further analytical insight into the shape of the tumour boundary can be gained by considering asymptotic limits of equation (65). For example, in the limit as $\mu(0) \to 0$, equation (65) reduces to give

$$\hat{A} = 1 - \frac{\eta}{\eta_1}, \qquad \text{where} \qquad \eta_1 = 2\mu(1)\lambda^{\frac{(4\mu(1)-\lambda)}{4\mu(1)}}.$$

Hence we deduce that when the surrounding fluid is inviscid and offers no resistance to tumour expansion, the profile of the surface $R(\eta) \sim (1 - \eta/\eta_1)^{1/2}$, with the position of the tip (where $\hat{A} = 0$) given by $\eta = \eta_1$ (hence, $S_S(t^*) = \eta_1 \exp(k_m(1)t^*)$ in agreement with (57)).

In this section we have used analytical methods to determine the large time behaviour of the tumour surface when the viscosity of the tumour and surrounding fluid differ. In the following section we consider the full model problem given by (11)-(14) and examine the stability of the interface.

5. Planar growth ($\lambda = 0$) and linear stability

5.1. One-dimensional solution

We define the one-dimensional variables for $v(r, z, t), u(r, z, t), p(r, z, t), n(r, z, t)$ and $s(r, t)$ to be $v_0(z, t)$, $u_0(z, t)$, $p_0(z, t)$, $n_0(z, t)$ and $s_0(t)$ respectively. When $\lambda = 0$ the tumour grows parallel to the duct wall axis so that $u_0 = 0$ and our nutrient-rich model (11)-(14) reduces to give

$$\frac{\partial n_0}{\partial t} + \frac{\partial}{\partial z}(n_0 v_0) = k_m(1)n_0, \tag{66}$$

$$\frac{\partial v_0}{\partial z} = k_m(1)n_0, \tag{67}$$

$$\frac{\partial p_0}{\partial z} = \frac{4}{3}\mu\frac{\partial^2 v_0}{\partial z^2}. \tag{68}$$

Solving equations (66)-(68) and the one-dimensional form of (29) (i.e. $ds_0(t)/dt = v_0$) with boundary conditions (16), and velocity and stress continuity conditions (25)-(26), gives

$$n_0 = \begin{cases} 1 \\ 0 \end{cases} \qquad v_0 = \begin{cases} k_m(1)z \\ k_m(1)s_0(t) \end{cases} \qquad p_0 = \begin{cases} 4\mu(1)k_m(1)/3 & 0 < z < s_0(t), \\ 0 & z > s_0(t). \end{cases}$$

with $s_0(t) = \exp(k_m(1)t)$. The cell velocity along the duct is continuous across the interface, increasing linearly with distance from the tumour centre ($z = 0$) inside the tumour, as the new cells migrate outwards. The velocity is constant in the surrounding fluid as no cells are dividing there. The right hand side of (68) is zero on either side of $z = s_0(t)$ but leads to a discontinuity in the pressure at the interface (see (26)). This is due to the volumetric source term (from cell division) in the stress condition, illustrating how cell proliferation (occurring only within the tumour) is responsible for producing the pressure field.

5.2. *Linear stability analysis*

5.2.1. *Moving boundary formulation and linearisation*

Following [14], [4] and [12], we can analyse the stability properties of the tumour growing inside the duct by applying small perturbations to the tumour surface. Adopting the discontinuous initial data (9), so that n is represented by a step function, we have equation (24) and from (23)

$$\nabla \cdot \mathbf{v} = \begin{cases} k_m(1) & 0 < z < s(r,t), \\ 0 & z > s(r,t). \end{cases}$$

We also have the kinematic condition (29) with the conditions for the radial and axial fluid velocities and stresses given by (10).

We perturb u, v, p and s by a small amount ($0 < \epsilon \ll 1$) such that

$$\begin{aligned} u &\sim \epsilon u_1(r,z,t), & s &\sim s_0(t) + \epsilon s_1(r,t), \\ v &\sim v_0(z,t) + \epsilon v_1(r,z,t), & p &\sim p_0(z,t) + \epsilon p_1(r,z,t). \end{aligned} \tag{69}$$

where v_0, s_0 and p_0 are the one-dimensional solutions and u_1, v_1, s_1 and p_1 are the two-dimensional perturbations. The perturbations then satisfy (assuming μ is piecewise constant)

$$\nabla p_1 = \mu \nabla^2 \mathbf{v}_1, \tag{70}$$

$$\nabla \cdot \mathbf{v}_1 = 0, \tag{71}$$

for $0 < z < \infty$, $0 < r < 1$ with boundary conditions (referring to (16))

$$\begin{aligned} &\text{on } z = 0 && \frac{\partial p_1}{\partial z} = 0, \quad \frac{\partial u_1}{\partial z} = 0, \quad v_1 = 0, \\ &\text{as } z \to \infty && p_1 = 0, \quad u_1 = 0, \quad \frac{\partial v_1}{\partial z} = 0, \\ &\text{on } r = 0 && \frac{\partial p_1}{\partial r} = 0, \quad u_1 = 0, \quad \frac{\partial v_1}{\partial r} = 0, \\ &\text{on } r = 1 && \frac{\partial v_1}{\partial r} = 0, \quad u_1 = 0. \end{aligned} \tag{72}$$

It remains to specify continuity conditions at the interface $z = s(r,t)$; these are derived as follows. Expanding (25)-(27) and (29) about s_0 to $O(\epsilon)$ we obtain the following conditions at $z = s_0$:

$$\left[p_1 + \frac{2}{3}\mu \left(\frac{\partial u_1}{\partial r} + \frac{u_1}{r} \right) - \frac{4}{3}\mu \frac{\partial v_1}{\partial z} \right]_-^+ = 0, \tag{73}$$

$$\left[\mu(0) \left(\frac{\partial u_1}{\partial z} + \frac{\partial v_1}{\partial r} \right) \right]^+ = \left[\mu(1) \left(2k_m(1) \frac{\partial s_1}{\partial r} + \frac{\partial u_1}{\partial z} + \frac{\partial v_1}{\partial r} \right) \right]^-, \tag{74}$$

$$\frac{\partial s_1}{\partial t} = v_1^+, \tag{75}$$

$$[v_1]_-^+ = k_m(1) s_1, \tag{76}$$

$$[u_1]_-^+ = 0. \tag{77}$$

To summarise, the corrections terms u_1, v_1, p_1 and s_1 are determined by equations (70), (71) and (75) subject to boundary conditions (72)-(74) and (76)-(77).

If we seek separable solutions of the form $u_1 = f(z,t)g(r)$, then after some algebra it is possible to show that u_1, v_1 and p_1 can be written as:

$$u_1^- = -\left\{\Gamma_0(t)\cosh(\alpha z) + \Gamma_1(t)\left(\frac{1}{\alpha}\cosh(\alpha z) + z\sinh(\alpha z)\right)\right\} J_1(\alpha r),$$
$$u_1^+ = \left\{\Gamma_2(t) + \Gamma_3(t)\left(z - \frac{1}{\alpha}\right)\right\}\exp(-\alpha z) J_1(\alpha r),$$

$$v_1^- = \{\Gamma_0(t)\sinh(\alpha z) + \Gamma_1(t) z\cosh(\alpha z)\} J_0(\alpha r),$$
$$v_1^+ = \{\Gamma_2(t) + \Gamma_3(t) z\}\exp(-\alpha z) J_0(\alpha r),$$

and

$$p_1^- = 2\mu(1)\Gamma_1(t)\cosh(\alpha z) J_0(\alpha r),$$
$$p_1^+ = 2\mu(0)\Gamma_3(t)\exp(-\alpha z) J_0(\alpha r),$$

where $\Gamma_i(t)$ $(i = 0, 1, 2, 3)$ are arbitrary functions of t which along with the perturbation to the surface $s_1(r,t)$ are determined by (73)-(77), $J_0(\alpha r)$ and $J_1(\alpha r)$ are Bessel functions of the first kind of zeroth and first order respectively, and the constant α solves $J_1(\alpha) = 0$ (this condition ensures that $u_1 = \partial v_1/\partial r = 0$ on $r = 1$). The large time behaviour of $s_1(r,t)$ is found to be

$$s_1 = s_{1_0}\exp\left(\frac{k_m(1)t}{1 + \frac{\mu(0)}{\mu(1)}}\right) J_0(\alpha r), \tag{78}$$

where the constant s_{1_0} is proportional to the initial amplitude. Hence, when $\lambda = 0$ and provided that $\mu(0)/\mu(1) > 0$, the perturbation to the planar surface grows, but at a slower rate than the leading order behaviour i.e. $s_0 \sim \exp(k_m(1)t)$ (note that we are perturbing a moving boundary rather than a fixed equilibrium solution). We observe that the perturbation to the surface grows most rapidly when $\mu(1) > \mu(0)$, that is when the tumour is more viscous than the surrounding fluid: this is also the case that is most physically relevant when considering DCIS because in general even though the bonds between malignant cells are fairly weak (compared to those of normal cells) it is reasonable to assume that they will be stronger than those holding the molecules together in the extracellular fluid.

5.3. Numerical solutions

To verify the long time predictions of the stability analysis when $\lambda = 0$, we examine the stability of the surface numerically. As described in Section 2.2, we solve equations (11), (15)-(18) with boundary conditions given by (16) and (20), but with the following initial condition for the tumour cell concentration

$$n(\mathbf{x}, 0) = \frac{1}{2}\left[1 - \tanh\{100\,(z - s(r,0))\}\right],$$

so that the tumour surface (i.e. where n falls rapidly from $n = 1$ to $n = 0$) has been perturbed. It should be noted that we have adopted a smooth function for n to enable us to solve the problem numerically, rather than a discontinuous step function as for the analysis. $s(r, 0)$ is defined by (69) where s_1 is given in (78). Earlier we determined that $J_1(\alpha) = 0$. We are interested in the fastest growing mode, hence α is taken to be the first zero i.e. $\alpha = 3.83171$. Figure 15 shows how the contours of the tumour cell concentration progress with time, while Figure 16 shows a direct comparison between the linear stability analysis and the numerical simulations. We observe from Figure 15 that the surface is unstable, with the perturbation to the interface growing at a rate consistent with the linear stability analysis (Figure 16) and more slowly than the advancing tumour. The differences in fingering at varying contours of n and the spreading of the front are accounted for by numerical diffusion and smoothed initial conditions. This is discussed in detail in [12] where a sensitivity study of the contours to initial conditions has been carried out.

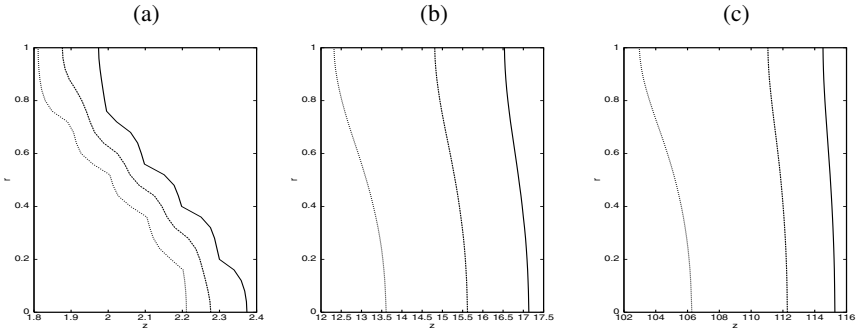

Fig. 15. Contours $n = 0.1$ (solid line), $n = 0.5$ (dashed line) and $n = 0.9$ (dotted line) at times (a) $t = 0$, (b) $t = 2$, (c) $t = 4$. $\lambda = 0$.

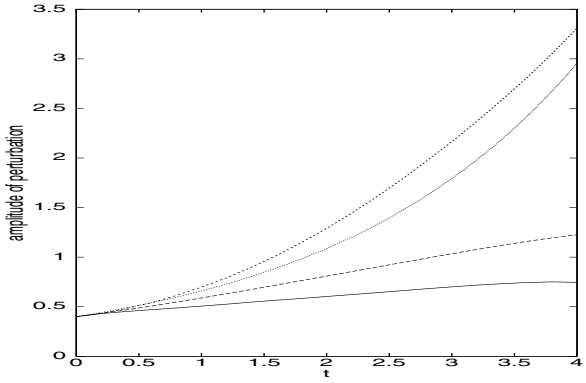

Fig. 16. Comparison of the results from the linear stability analysis (small dotted line) and the numerical simulations (contours $n = 0.9$ (dotted line), $n = 0.5$ (dashed line) and $n = 0.1$ (solid line)) for the rate of growth of small perturbations to the surface with $\alpha = 3.83171$ and $\lambda = 0$.

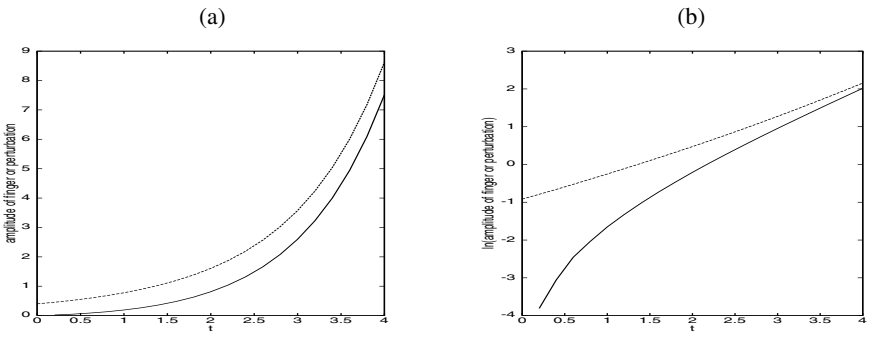

Fig. 17. (a) The amplitude of the perturbation for contour $n = 0.5$ for planar front initial conditions (solid line) and perturbed initial conditions (dashed line). (b) The log plot of (a). $\lambda = 0.1, \alpha = 3.83171$.

We now consider the case when $\lambda \neq 0$ and hence the surface is no longer planar (it is difficult to make analytical progress in this case). Figure 17 shows a comparison between two simulations; the first is that when the tumour surface is flat initially and the second is when a perturbation has been applied to the surface. Figure 17(b) clearly shows that although the amplitudes of the perturbation or finger differ for small times, they grow at the same rate at later times. This implies that the surface is stable to small perturbations when $\lambda \neq 0$ and suggests that the finger-like shape of the tumour front is the stable configuration.

6. Conclusions

In this paper, the growth of a tumour in an two-dimensional axisymmetric cylindrical rigid duct has been examined in order to describe the initial stages of ductal carcinoma in situ. We have introduced a nutrient-limited growth model and have used Stokes flow to describe the movement of the cells. This modelling results in a system of nonlinear partial differential equations involving the surrounding fluid and the live and dead tumour cell concentrations, the nutrient concentration, the local velocity and the pressure. These were solved using numerical, asymptotic and linear stability techniques.

The numerical simulations in Section 2.3.2 suggest that because the cells are always a fixed distance away from the nutrient source (the duct is rigid), only a small number of cells die in the centre (mainly due to apoptosis). This suggests that growth in a nutrient rich environment may be sufficient to model these initial stages of DCIS with the nutrient-limited model becoming more relevant in the later stages where the duct wall is compliant and starts to deform. Since changing the consumption rate is equivalent to changing the diameter of the duct, it follows that for a duct with a larger radius, more nutrient is consumed and therefore more cells die in the centre of the duct. This goes some way to explaining why in high grade DCIS, where the duct is large and distended, a necrotic core is seen and why one is not observed in low grade DCIS.

The tumour cells adhere to the duct wall (although it is not known to what extent) and numerical simulations and asymptotic analysis for large time show that the more the cells are able to slip against the wall, the flatter is the surface of the tumour. The viscosity of the tumour and surrounding material also affects the shape of the tumour surface. By considering the case when the tumour is much longer in the axial direction than the radial direction in Section 4, we find that the tumour expands faster when the viscosity of the tumour is greater than the fluid because the surroundings are providing less resistance to growth. The tumour leaves the duct wall further along the duct as the tumour viscosity increases because the strength of the bonds between the cells is greater, meaning that the tumour is held together and to the wall more strongly. The tip of the tumour grows at a rate dependent upon the viscosity of the surrounding fluid so that as this increases, the position of the tip extends further along the duct. The shape of the tumour boundary therefore alters depending upon the relative viscosities but the tumour is growing at a constant rate regardless of the viscosity ratio so that the volume of the tumour remains constant.

In Section 5.2, the stability of the tumour surface was found to be dependent upon how the cells stick to the duct wall. If the front is planar (the cells slip against the wall) the surface is unstable to small perturbations. If however the cells stick to the wall (the front is more finger like), the perturbations decay so that the surface is stable. The linear stability analysis also suggests that the rate of growth of the perturbation to the surface does not depend upon the viscosity of the tumour and surrounding fluid.

In conclusion, we have developed a mathematical model describing the growth of an avascular tumour in a rigid cylindrical duct that incorporates the interaction between the tumour cells and the duct wall. We have observed that for all viscosities and nutrient concentrations, the pressure increases rapidly in the centre of the tumour suggesting that this may be the mechanism that causes the duct wall to deform i.e. it may eventually become easier for cells at the tumour centre to push against the compliant duct wall rather than push against other cells to spread further down the duct. Future work will examine the case when the wall is compliant, including a mechanism for degradation of the membrane due to the production of proteolytic enzymes. This may then lead on to an investigation of the invasion of the tumour into the surrounding breast tissue.

Acknowledgements. This work was funded in part by the EPSRC through a ROPA award (SJF) and an Advanced Fellowship (HMB).

References

1. Batchelor, G.K.: An introduction to fluid mechanics. Cambridge University Press, Cambridge, 1967
2. Breward, C.J.W., Byrne, H.M., Lewis, C.E.: Modelling the interactions between tumour cells and a blood vessel in a microenvironment within a vascular tumour. Eur. J. Appl. Math. **12**, 529–556 (2001)

3. Brummer, O., Athar, S., Riethdorf, L., Loning, T., Herbst, H.: Matrix-metalloproteinases 1, 2 and 3 and their tissue inhibitors 1 and 2 in benign and malignant breast lesions: an in situ hybridization study. Int. J. Path. **435**, 566–573 (1999)
4. Byrne, H.M.: The importance of intercellular adhesion in the development of carcinomas. IMA J. Math. Appl. Med. Biol. **14**, 305–323 (1997)
5. Byrne, H.M., Chaplain, M.A.J.: Growth of nonnecrotic tumors in the presence and absence of inhibitors. Math. Biosci. **130**, 151–181 (1995)
6. Byrne, H.M., Chaplain, M.A.J.: Growth of necrotic tumors in the presence and absence of inhibitors. Math. Biosci. **135**, 187–216 (1996)
7. Byrne, H.M., Chaplain, M.A.J.: Modelling the role of cell-cell adhesion in the growth and development of carcinomas. Math. Comput. Model. **24**, 1–17 (1996)
8. Byrne, H.M., King, J.R., McElwain, D.L.S., Preziosi, L.: A two-phase model of solid tumour growth. Appl. Math. Lett. In press
9. Chaplain, M.A.J., Sleeman, B.D.: Modelling the growth of solid tumours and incorporating a method for their classification using nonlinear elasticity theory. J. Math. Biol. **31**, 431–473 (1992)
10. Engels, K., Fox, S.B., Whitehouse, R.M., Gatter, K.C., Harris, A.L.: Distinct angiogenic patterns are associated with high-grade in situ ductal carcinomas of the breast. J. Path. **181**, 207–212 (1997)
11. Fernandez-Gonzalez, R., Jones, A., Garcia-Rodriguez, E., Chen, P.Y., Indica, A., Lockett, S.J., Barcellos-Hoff, M.H., Ortiz de Solorzano, C.: System for combined three-dimensional morphological and molecular analysis of thick tissue specimens. Microsc. Res. Techniq. **59**, 522–530 (2002)
12. Franks, S.J.: Mathematical modelling of tumour growth and stability. PhD Thesis, 2001
13. Greenspan, H.P.: Models for the growth of a solid tumor by diffusion. Stud. Appl. Math. **51**, 317–340 (1972)
14. Greenspan, H.P.: On the growth and stability of cell cultures and solid tumors. J. Theo. Biol. **56**, 229–242 (1976)
15. Hanby, A.M., Millis, R.R., Oberman, H.A.: Diagnostic surgical pathology. Lippincott Williams and Wilkins, Philadelphia, 1999
16. King, J.R., Franks, S.J.: Mathematical analysis of some multi-dimensional tissue-growth models. Submitted, 2002
17. Landman, K.A., Please, C.P.: Tumour dynamics and necrosis: surface tension and stability. IMA J. Math. Appl. Med. Biol. **18**, 131–158 (2001)
18. Moore, J.V.: Death of cells and necrosis in tumours: Perspectives in Mammalian Cell Death. Oxford University Press, Oxford, 1987
19. Morton, K.W., Mayers, D.F.: Numerical solution of partial differential equations. Cambridge University Press, Cambridge, 1994
20. Mueller-Klieser, W.F., Sutherland, R.M.: Oxygen-tensions in multicell spheroids of 2 cell-lines. Br. J. Cancer **45**, 256–264 (1982)
21. Please, C.P., Pettet, G.J., McElwain, D.L.S.: Avascular tumour dynamics and necrosis. Math. Mod. Meth. Appl. Sci. **9**, 569–579 (1999)
22. Ward, J.P., King, J.R.: Mathematical modelling of avascular-tumour growth. IMA J. Math. Appl. Med. Biol. **14**, 39–69 (1997)